

Comparison of Topographic and Physiographic Properties Measured on the Ground with Those Derived from Digital Elevation Models

Abstract

With the widespread availability of digital elevation models (DEM) and regional surveys of soils, topographic and physiographic features of landscapes are now more easily characterized. Within southwestern Oregon 391 field plots were registered within a geographic information system (GIS) to digitized topographic and soils coverages and properties extracted from the digital coverages compared with those estimated in the field. The initial comparison showed major differences in estimates of aspect, slope, and maximum available soil water content (θ), although the location of plots showed general agreement with elevations recorded on the maps. To extrapolate climatic data and interpret hydrologic responses accurately, an automated search procedure was developed whereby the initial location of each plot was, if necessary, shifted within specified bounds to give closer agreement with field estimates of aspect, slope, and θ . Specifically, the search routine sequentially identifies the nearest 100 m-resolution cell within a search radius of 3 or 5 cells in which differences are within $\pm 22.5^\circ$ of aspect, $\pm 20\%$ of slope, and in closest agreement with field estimates of θ . The search procedure resulted in improved agreement with field estimates: $r^2 = 0.82$ for aspect, 0.56 for slope, 0.54 for θ . To obtain these improvements required that the initial plot locations be shifted, on the average, 289m within the 3-pixel search radius, and 435 m within the 5 pixel radius. With the terrain analysis procedures developed in this paper, it is possible to overcome many problems associated with registering the precise location of field plots upon digitized topographic and soil maps. The procedure is particularly appropriate in situations where the environmental regimes associated with a specified field location are to be extrapolated across landscapes. The approach also permits a wealth of historical survey plot data to be incorporated into a GIS format and to be spatially extended.

Introduction

Basic information on geographic location, elevation, slope and aspect are collected in most soil and vegetation surveys. Additionally, soil properties are often characterized to provide estimates of maximum available soil water storage in mm (θ) and drainage conditions. Indirectly, these topographic and physiographic features affect the growth and distribution of vegetation as well as the hydrologic response of landscapes to precipitation (Running et al. 1989; Running 1994; Waring and Running 1998). Although soil surveys generally provide broad estimates of θ , a number of studies have demonstrated that local spatial variation of topographic features helps to explain much of the variation in soil water capacity (50m to 200 m) (Band 1986; Band et al. 1993; Nemani et al. 1993). Compared to traditional methods of estimating θ from soil series data, estimates derived from digital elevation models (DEM) provide additional information because topographic data are collected at higher resolution than soil series data.

The possibility of spatially classifying estimates of terrain variability within a digital environment has become possible with the development of ter-

rain analysis programs and DEMs. The general trend in representations of terrain for environmental modelling has been to move from broad, continental and regional scales, to finer scales more suited to the modelling of surface hydrology, vegetation and soil properties. This trend can be attributed to improvements in methods for representing fine scale topographic shape and structure, supported by the steady increase in the speed and storage capacity of computing platforms.

Fine scale DEMs, with spatial resolutions from 5 to 100 m, are typically used for spatially distributed hydrological modelling (Binley and Beven 1992, Zhang and Montgomery 1994) and for the analysis of soil properties (Gessler et al. 1996). The determination of appropriate spatial scales for hydrological modelling is an active research issue (Bloschl and Sivaplan 1995). Terrain attributes can be referred to as DEM derivatives as their calculation is based upon first-order and second-order derivatives of a continuous 3-D surface. The surface can be based on a combination of discrete tiles, grids, or triangular regular networks (TINs), or contour segments. In any case, the algorithms are approximations of those for continuous surfaces. Moore et al. (1991) reviewed the applications of digital terrain modeling and

listed the major primary terrain attributes that could be derived from a DEM and their application.

Grid based DEMs are developed directly from standard digital topographic data which may include spot heights, elevation contours, stream lines and dams and lakes. The method produces DEMs which respect surface shape and drainage. It can use stream line data, without associated elevation data, to aid the representation of surface drainage. The ready availability of DEMs does not imply however, that they are without error and often are not always available at the most appropriate scale (Hutchinson 1999). In addition, there are a number of potential errors associated with DEMs that are independent of scale:

- (a) coastal and flat areas may be represented as terraces due to slope calculations made where flat areas alternate with narrow bands of steeper slopes.
- (b) interpolation errors may result over surfaces caused by methods failing to interpret contour data correctly.
- (c) local peaks not modeled at their correct height and will appear to be flattened due to poor placement of base spot height data.
- (d) offsets related to slope direction and steepness on one side of a topographic feature will result in an overestimate of elevation on one side and an underestimate on the other.

Linking historical data collected at specific points within the DEM requires adjusting for errors that may occur in assigning the initial location of plots to maps that differ in accuracy from those now available and were located without global positioning satellite (GPS) technology. Fortunately, it is now possible, using automated searching logic to examine the geographic position of each plot location with respect to its local terrain and predict its most likely geographic position on current DEMs.

The objective of this paper is to present an approach which compares plot-based measurements of terrain variables with calculations made from a 100 m-resolution DEM and employs an algorithm that searches, within a defined radius, DEM cells to predict the most likely position of the plot within the landscape. Once located, estimates of slope and aspect are extracted from the DEM and θ is predicted with a generalized model derived from topographic and soil series data.

Study Area and Data

The region of southwest Oregon lying between the southern Cascade Mountains and Pacific Coast is an area of great diversity in climate, geology, and vegetation. The developing patterns in vegetation differ, depending on the topographic location and differences in parent material. At lower elevations near the coast, Port-Orford cedar (*Chamaecyparis lawsoniana* (A. Murr.) Parl.) and Douglas-fir (*Pseudotsuga menziesii* (Mirb.) Franco) are common on moist sites. At higher elevation where a winter snowpack accumulates, Shasta red fir (*Abies magnifica* var. *shastensis* Murr. Lemm.) and mountain hemlock (*Tsuga mertensiana* (Bong.) Carr.) dominate. At mid-elevations on drier sites, Douglas-fir is often accompanied by tanoak (*Lithocarpus densiflorus* (Hook. & Arn.) Rehd.), western white pine (*Pinus monticola* Dougl. ex D. Don) and sugar pine (*Pinus lambertiana* Dougl.). On the most extreme sites with shallow soils or inhospitable parent materials derived from serpentine or peridotite, ponderosa pine (*Pinus ponderosa* Dougl. ex Loud), canyon live oak (*Quercus chrysolepis* Liebm.) and Jeffrey pine (*Pinus jeffreyi* (Grev. and Balf.) are present (Whittaker 1960, Franklin and Dyrness 1973).

Plot Data

From 1981 to 1983 a series of temporary plots were established as a forest growth modeling project within the southwest Oregon Forestry Intensified Research Program (Hann and Ritchie 1988, Hann and Wang 1990, Hann and Larsen 1991). A total of 384 forest stands ranging in size from 2 to 47 ha were selected for field sampling. A total of 391 temporary research plots were established in these stands covering an area of 54,000 km². The research plots were placed in a cluster design of 4 to 10 sampling units over 1.5 to 4 ha. A modal soil pit was dug at the sampling unit judged to be the most representative of the cluster based on soil attributes. The aspect and slope were measured and the depth and soil texture described by horizons down to 1.4 m or to bedrock were recorded. The maximum available soil water content (θ) was estimated by accounting for variation in soil texture and rock content down to the maximum defined depth (Hann 1983). The geographic location and elevation of each plot was estimated from U.S.G.S. 15 minute topographic maps. For the remainder of this paper, the slope,

aspect, elevation and geographic position of the sampling unit which contained the soil pit will be used to represent the plot as a whole.

DEM Data

Digital elevation data for southwestern Oregon were obtained from the Defense Mapping Agency (DMA, Portland Oregon) with an initial pixel resolution of 80 m. The data were then rectified to 100-m pixel resolution and registered on the Universal Transverse Mercator map projection. A general description of the DEM properties is presented in Table 1.

TABLE 1. Properties of the Digitized Elevation Model for Southwestern Oregon.

Position	Easting	Northing	Cell size (m)
Top Left	305500	4805000	100
Bottom Right	598000	4640000	100

A number of terrain attributes were calculated from the DEM surface. The first and simplest variable to extract was site elevation. The slope of each pixel was calculated by fitting a plane to the difference in elevation between a central cell and the immediately adjacent 3 X 3 array of 100 m cells. The direction that the plane faced defined the aspect for the central cell following the average maximum technique described by Zevenbergen and Thorne (1987) and Moore et al. (1991). To define the direction of water flow through the central cell, the steepest descent of each cell in the 3 X 3 array was estimated following the methods of Jenson and Domingue (1988). The flow accumulation was calculated on a cell by cell basis to take account of the total up-slope area that drained into and through a selected central cell.

The Compound Topographic Index (CTI) (unitless) was computed as a function of the contributing area up-slope of a central cell and the slope at that central cell (Moore et al. 1991). The CTI is calculated as:

$$CTI = \ln\left(\frac{\alpha}{\tan(\beta)}\right) \quad (1)$$

Where α is the up-slope contributing area and β is the slope.

In areas with negligible slope, a CTI value of 0.001 was assigned. This value is smaller than that obtained from a 100 m data set differing in

elevation by 1 m. The CTI was originally used in hydrologic models for small basins with high values indicating a greater likelihood of a saturated contributing area (Kirkby and Weyman 1974, Beven and Kirkby 1979; Beven and Wood 1983). The higher values of CTI tend to be found at the lower parts of watersheds and in convergent hollow areas associated with soils of low hydraulic conductivity or areas with more gentle slope than average (Beven and Wood 1983). Soil depth and silt and clay content tend to increase from ridge tops to the valley bottoms (Singer and Munns 1987). Soil erosion is also related to the direction of water flow, with the rates highly dependent upon the degree that soils remain saturated (Zheng et al. 1996).

Soils Data

There is a wide variety information on soils available at varying spatial scales. Within the United States, the U.S. Department of Agriculture's (USDA) Natural Resources Conservation Service (NRCS), formerly the Soil Conservation Service (SCS), leads the National Cooperative Soil Survey (NCSS) and is responsible for collecting, storing, maintaining, and distributing soil survey information for privately owned lands in the United States.

For regional scale mapping and monitoring the State Soil Geographic (STATSGO) data base is the most appropriate because it has been compiled at a consistent scale for all of the United States (United States Department of Agriculture 1991). STATSGO soil data are compiled from more detailed State Survey Geographic Data Base (SSURGO) soil survey maps and information on geology, topography, climate, and vegetation, supplemented by images derived through remote sensing from satellites. Using the United States Geological Survey's (USGS) 1:250,000 scale, 1-by 2-degree quadrangle series as a map base, the soil data are digitized as line segments to comply with national guidelines and standards. STATSGO soil data are often inadequate for local or even regional modeling, especially in mountainous areas. These inadequacies reflect the variation present within cells, insufficient sampling of each mapping unit, and difficulty of drawing boundaries between two different mapping units (Burrough 1986, Mark and Csillag 1990). Never the less, the STATSGO data base provides the only available

state-wide mapping of soil attributes carried out in a consistent manner.

For each soil series, the thickness of each soil horizon and its mean available soil water capacity was computed and summed for the entire profile to provide an estimate of θ for each polygon. This vector coverage was then converted to raster format with a spatial resolution (size of the cell) of 250 m, approximately equivalent to a 1:250,000 scale. If an individual cell was composed of polygons representing more than one soil series, the spatially dominant series was selected.

Soil Water Model

Although it was possible to develop regressions between field estimates of θ and those interpreted from the STATSCO data set, there are advantages in attempting to predict θ directly from hydrological models. First, regression relationships cannot be used in regions where STATSCO data are not available and second, static models make it difficult to assess the dynamic impact of large storms and the implications of road building and other activities on water movement. Zheng *et al.* (1996) proposed a simple model to estimate θ using the mean values of θ from the STATSCO data set to transform the fine-scale variation defined with the CTI. Equation 2 shows that a general positive relationship exists between CTI and θ (in mm) such that:

$$\theta = \{M_1, M_2\} \cdot \ln\left(\frac{\alpha}{\tan(\beta)}\right) \quad (2)$$

where M_1 and M_2 are case-specific coefficients, one of which is chosen for each pixel. Zheng *et al.* (1996) showed that the distributions of the calculated CTI when compared to θ as obtained from STATSCO datasets were always smaller with longer tails in the high end. Thus, two scalars are needed to avoid transforming right-skewed distributions of CTI into right-skewed distributions of θ . When a pixel's CTI value is less than or equal to its mean, the coefficient M_1 is used in Equation 2. M_1 is determined in equation 3 by:

$$M = \frac{\theta_{(STATSCO)me}}{0.5 \cdot (CTI_{mo} + CTI_{mean})} \quad (3)$$

where CTI_{mo} and CTI_{mean} are mode and mean values of the calculated CTI, respectively and $\theta_{STATSCO}$ is the mean value θ for a given spatial extent, estimated from either the mean of the

STATSCO θ or other relevant data. The function of M_1 is to re-scale the CTI values that are less than or equal to its mean at a rate for which the median value of CTI is equal to $\theta_{STATSCO}$.

When a pixel's CTI value is greater than its mean, the coefficient M_2 is used in Equation 2 and is estimated by equation 4:

$$M_2 = \frac{\theta_{(STATSCO)max}}{CTI_{max}} \quad (4)$$

where $\theta_{(STATSCO)max}$ is the maximum θ occurring in the STATSCO database for the region and CTI_{max} is the maximum CTI value with an occurrence rate at least 1%. Again, θ_{max} can be estimated for a given spatial extent from maximum STATSCO layer or from other relevant data. The function of M_2 is to re-scale CTI values that are larger than the CTI mean at the rate that makes the defined maximum CTI value equal to θ_{max} .

In this study, M_1 for Southwestern Oregon (100-m pixel resolution) was $17.4 / (0.5 * (3.8 + 1.3)) = 6.8$. The maximum calculated CTI value with an occurrence rate of over 1% was determined to be 16.3. A value of 40 cm was used for the maximum θ from STATSCO to determine M_2 for Southwestern Oregon. These different maximum values are close to the maximum value of θ estimated from field surveys (Table 2).

TABLE 2. Summary of input data used in the search routine to re-position field plots.

Data set	CTI	STATSCO (θ) (mm)	Plot Data (θ) (mm)
Pixel Resolution (m)	100	250	-
Number Plots	-	-	391
Number Polygons	-	1314	-
Number Pixels	3304394	-	-
Mean	3.8	168	174
Maximum	24	400	269
Minimum	0	0	39
Mode	1.3	51	157

GIS Search Algorithm

An initial test of the accuracy of the initial plot positions and the compatibility of the elevation, slope, and aspect data with the cell-based predictions was completed for all 391 plots. Based on this initial comparison, a search algorithm was developed to interrogate individual pixels within

a specified rectangular subset of cells (known as a boxcar) that exhibit similar slope, aspect, and θ attributes as those recorded in the field.

If each plot was located accurately, and the terrain attributes were all calculated without error, then the central pixel in the boxcar would share all the attributes recorded at the field plot, a situation that rarely happens.

The formal computation presented in the algorithm can be described in equation 5.

$$W(P)_{ij} = \min_{n=1}^{n=m} |P(\text{Aspect}, \text{Slope}, \theta)_{ij} - P(\text{Aspect}, \text{Slope}, \theta)| \quad (5)$$

where W_{ij} is the re-computed geographic position of plot P, $P(\text{Aspect}, \text{Slope}, \theta)_{ij}$ are the terrain

attributes for the cell coincident with the original plot location on the DEM, and $P(\text{Aspect}, \text{Slope}, \theta)$ is the aspect, slope and θ , as recorded in the field at the plot location. The search is undertaken for all cells from $n = 1$ to $n = m$ where m is the number of cells.

The operational steps are shown diagrammatically in Figure 1 and are applied for each plot as follows:

- Initially, the plot aspect is compared to the aspect of all cells in a specified boxcar filter. If any cells have aspects that lie within $\pm 22.5^\circ$, the cells are tagged as acceptable candidates.

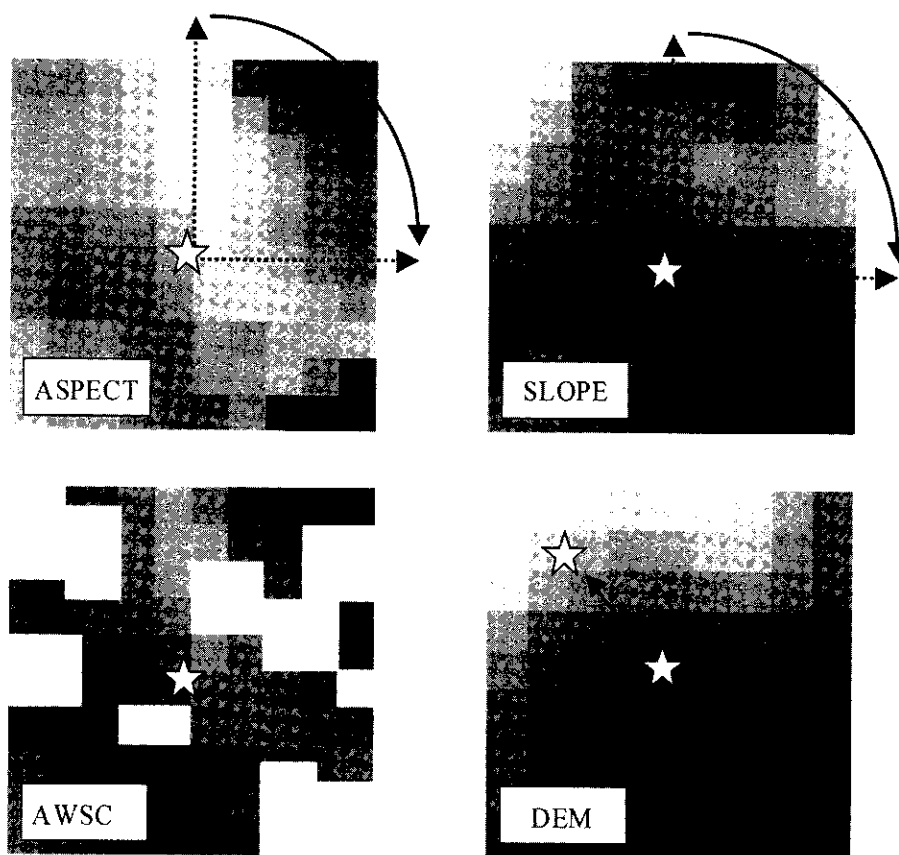


Figure 1. Procedures for selecting cells with attributes in closest overall agreement to those described from field measurements. Plot centre is indicated by star with the search routine moving in a clockwise direction as indicated arrows. The sequence from upper left to lower right is hierarchical: (1st) aspect, (2nd) slope, (3rd) θ , and finally, repositioning of the plot. AWSC: Available Water Soil Capacity; DEM: Digital elevation model.

- This process is repeated on the slope layer with cells having values within $\pm 20\%$ of the plot slope being tagged as acceptable candidates.
- All cells in the search region are then ranked based on the above classifications, with cells having two successful passes (i.e., both aspect and slope being within the specified thresholds) ranked the highest (code 3), followed by plots with aspects within specific thresholds but not slopes (code 2), cells with slopes correct but not aspect (code 1), and finally cells where neither the DEM slope nor aspect lays within the specified thresholds.
- Only cells with the maximum code are kept; all other cells are discarded. For all remaining possible candidates, the predicted θ of each cell is extracted and compared to the value of θ recorded at the plot. The cell with the highest code based on aspect and slope suitability and the smallest absolute difference between θ predicted by the DEM and measured in the field was then selected as the new plot position.

Implicit in this approach is a hierarchy in the application of the thresholds with plot aspect in this project selected as the most important terrain variable to match. This is primary due to the strong effect of aspect on radiation, especially at sites with high latitudes. For example, the incorrect positioning of the plot location based on aspect by locating it on an exposed rather than protected aspect, can have a major effect on its correct environmental description.

In this implementation, aspect and slope are first matched with the plot estimates. The comparison of θ is only undertaken in the final phase. As a result, if cells surrounding the original plot position have predicted θ values identical to those measured in the field and the slope and aspects do not lie within the selected thresholds, the cells are not candidates for plot selection.

The GIS-search algorithm was implemented at 2-boxcar filter sizes, the first with a maximum boxcar filter of 5 pixels from the plot center (equating to a maximum radius of 848 m from the original plot position) and a second, more conservative search limit with a maximum of 3 pixels from the plot center (equivalent to a maximum radius of 565 m from the original plot position). Statistical analysis was undertaken in the STATISTICA software package (StatSoft 1995).

Results

Extremes in elevation extracted from the DEM (with a cell resolution of 100 m) over the study area range from sea level (0 m) to 2840 m with a mean elevation of 850 m and a standard deviation of 507 m. This can be compared to the highest elevation in the study region (Mt. McLouglin at 2894m ASL). Figure 2(a) shows the frequency distributions of the field measured slopes of the 391 plots and the slopes extracted for the cells corresponding to the original plot positions. Figure 2(b) shows the frequency distribution of aspects for the 391 plots and the aspects extracted for all corresponding cells.

The two aspect distributions show similar trends with 1 or 2% differences in the number of plots in each of the 16 categories of aspect. Both distributions indicate that there are fewer plots located in an easterly than westerly direction. The most common field measured aspect was in a southerly direction, while the maximum number of cells from the DEM are located in northerly directions. The slope distributions are distinctly different with large variations in the number of plots in each of the slope-percentage classes. A major effect of the 100 m spatial resolution of the DEM is to impose a smoothing function on its representation of terrain, which results in many high frequency spatial features such as ridges and gullies being smoothed by the DEM algorithm at the 100 m cell scale. Consequently, slopes computed from the DEM are less steep than those measured in the field. Thus in Figure 2a DEM cells have slopes greater than 60 % yet 3 % of the 391 field plots have slopes exceeding 60 %. Therefore, there is a much greater percentage of cells from the DEM plots in the lower slope classes than estimated at each plot.

A Kolmogorov-Smirnov statistic provides a method to verify the similarity of the two distributions by testing if the samples are representative of the same distribution. The Kolmogorov-Smirnov assesses the hypothesis that two samples (the field data and the data extracted from the DEM) were drawn from different populations. The test is sensitive to differences in the general shapes of the distributions in the two samples and if the test is statistically significant results in the rejection of the hypothesis that the DEM data matches the field observations (Kolmogorov 1941). The test indicates that the distributions and the variances

(a)

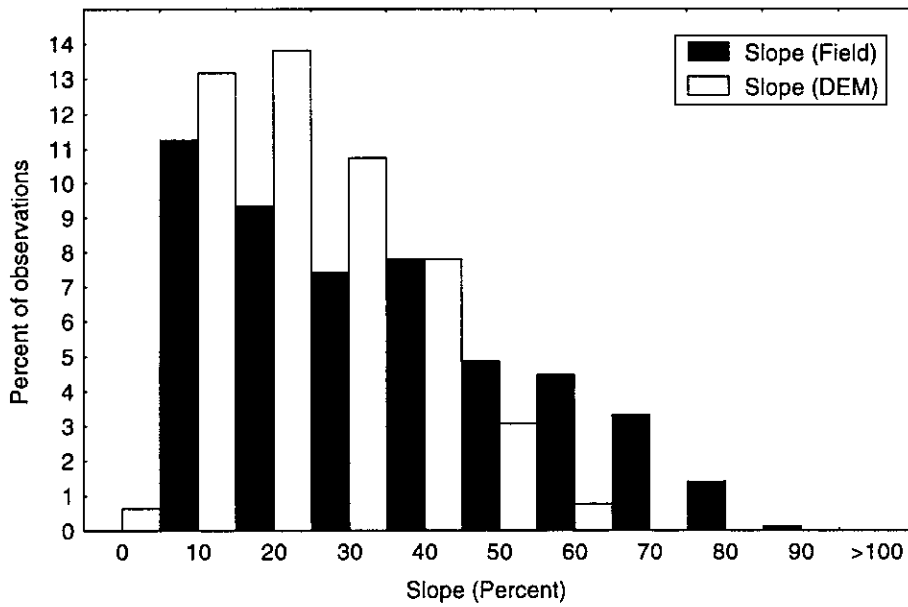


Figure 2a. Frequency distributions of slopes as measured in the field at their original locations and those derived from DEM.

(b)

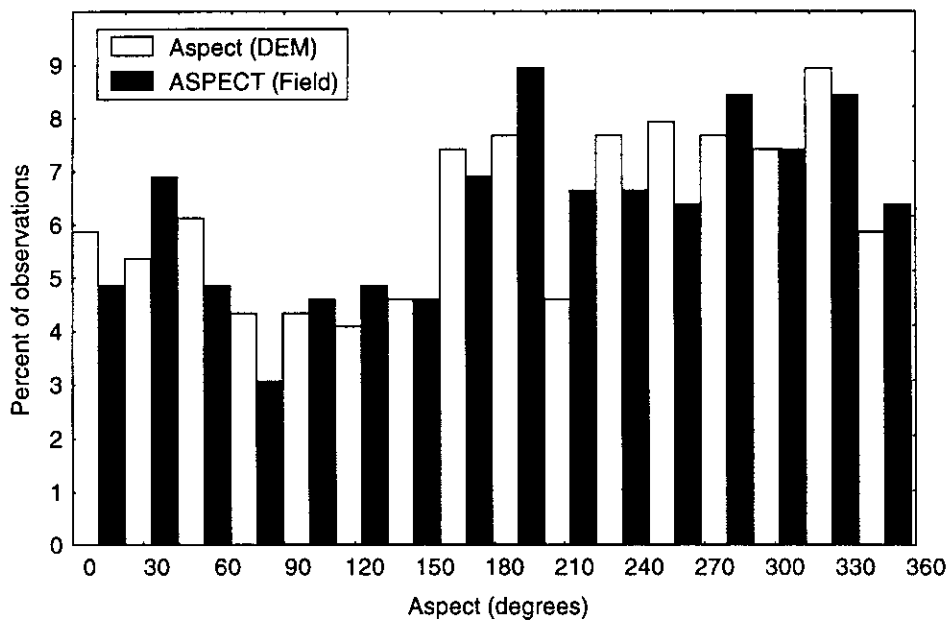


Figure 2b. Frequency distributions of aspect as measured in the field at their original locations and as derived from DEM.

of the DEM and plot data for both slopes and aspects are significantly different at the 0.05 level, with the differences in slope distributions and variances being highly significant ($P < 0.01$).

Figure 3a shows the field estimates of elevation (in meters) plotted against the elevation of the 391 cells correspond closely to values measured at the original plot locations. Figure 3b shows

the field estimates of aspect (in degrees) plotted against the aspect of the 391 cells recorded at the original plot locations and Figure 3c for the slope estimates (in percent). These results indicate that while the elevations are in good agreement, the correspondence of DEM estimates of the slopes and aspects with data recorded at the 391 plots is poor, particularly for the latter attribute.

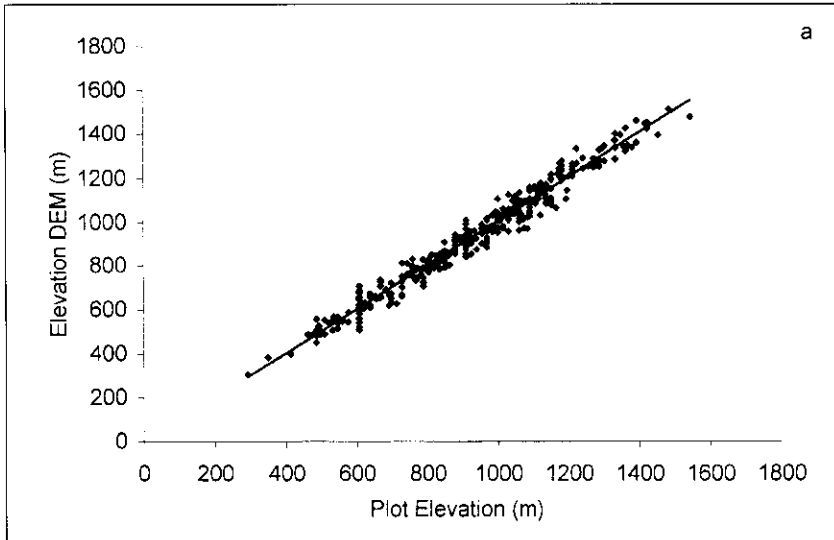


Figure 3a. Relationship between elevation recorded at the original locations in the field and that predicted with the DEM ($r^2 = 0.97$, DEM Elevation = $1.0 * \text{Plot Elevation} - 0.02$, $n=391$, $P < 0.0001$)

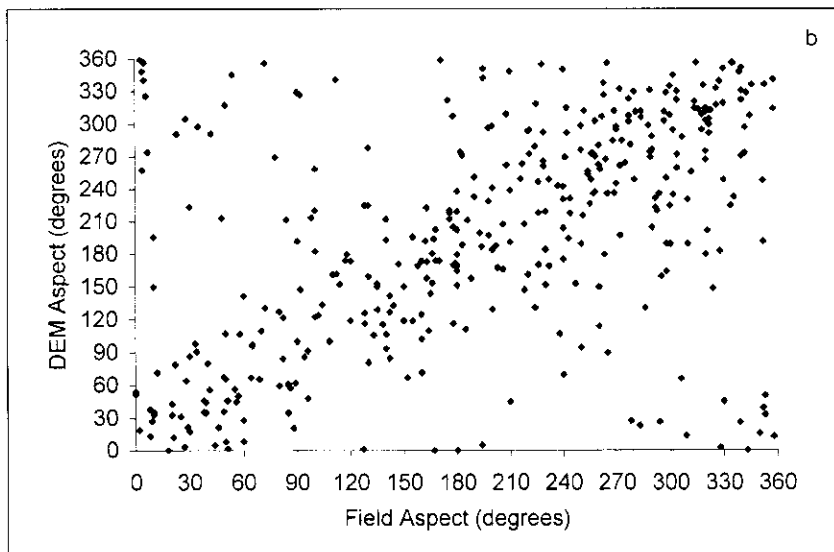


Figure 3b. Relationship between aspect recorded at the original locations in the field and that predicted with the DEM ($r^2 = 0.23$, DEM Aspect = $0.49 * \text{Plot Aspect} + 94.6$, $n=391$, $P < 0.0001$)

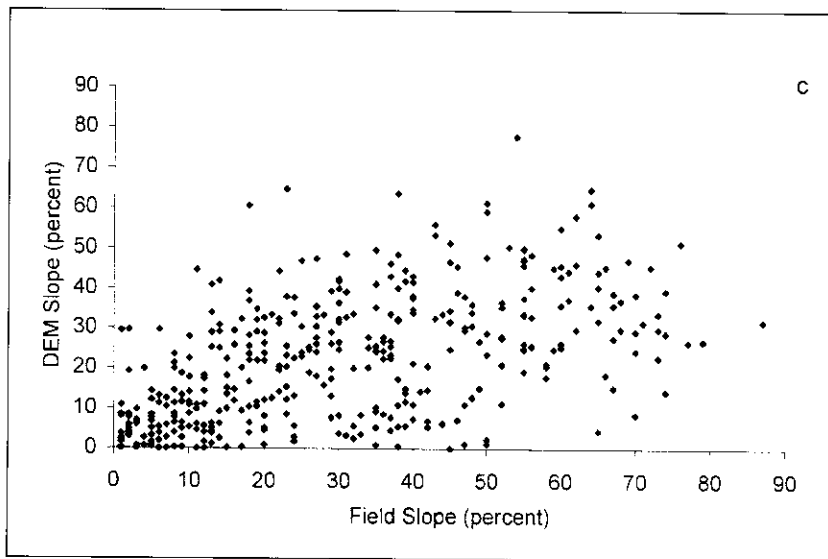


Figure 3c. Relationship between slope recorded at the original locations in the field and that predicted with the DEM ($r^2 = 0.30$, DEM slope = $0.42 * \text{Plot Slope} + 9.1$, $n=391$, $P < 0.0001$)

The good agreement between the elevations recorded at the plots and those extracted from the DEM indicate that, while the geographic location of the plots and the terrain cells may not directly correspond, the locations are generally within close proximity, and differences are mainly associated with local variations in slope and aspect.

Figures 4a and b show the relationship between the field aspects and DEM aspects in the new positions determined with the GIS-search algorithm. Two sets of results are presented using the 3- and the 5-pixel-radius-search boxcar filters. The figures show the hierarchy of the search procedure with the code 3, 2, and 1 results represented as different symbols. In a number of cases, the plot measured aspect and slopes could not be matched to any cells in the DEM search filters. In the 5 pixel radius, 3.3% of plots ($n=13$) could not be matched, with 3.6 % unmatched ($n=14$) using the 3 pixel radius. As a result, these plots were removed from the dataset and are not included in the presentation of the results.

Figures 4c and d show the relationship between the field slopes and the slopes of the DEM cells in the new positions determined using the GIS search algorithm. Again both sets of searches are presented and the figures show the hierarchy with the code 3, 2 and 1 identified. Figures 4e and f shows the predicted versus measured θ as extracted

at new plot positions for both the 5- and 3-pixel-boxcar-search windows.

Figure 4a and b show that there is a significant increase in the correspondence between aspect measured at the plot and that at the repositioned plot locations extracted from the DEM. In the case of 5-pixel radius, the majority of the plots (84%) have been coded 3, which indicates that both the slope and the aspect of the repositioned plots were within the slope and aspect threshold classes. Additionally, 8% of plots were coded 2 which indicates aspect of the repositioned plots were within the threshold established although no cells with slopes within the prescribed threshold could be located. Because of the 360° representation of aspect, values $< 22.5^\circ$ or $> 347.5^\circ$ transfer to the NE or NW quadrants; This results in their location appearing to be more erroneous than is actually the case on the scatter plot.

The distribution of plots with code 1 (plots with slope within the slope thresholds but no agreement with aspect) appears to be random over the range of aspect indicating that, in spite of matching slopes, there was a continual mismatch at some plots. The results of the larger search window (5 pixels) is a tighter clumping of the measured versus predicted aspects along the 1:1 line with more cells classified as code 3 and less as code 2 than resulted with the more conservative window. The

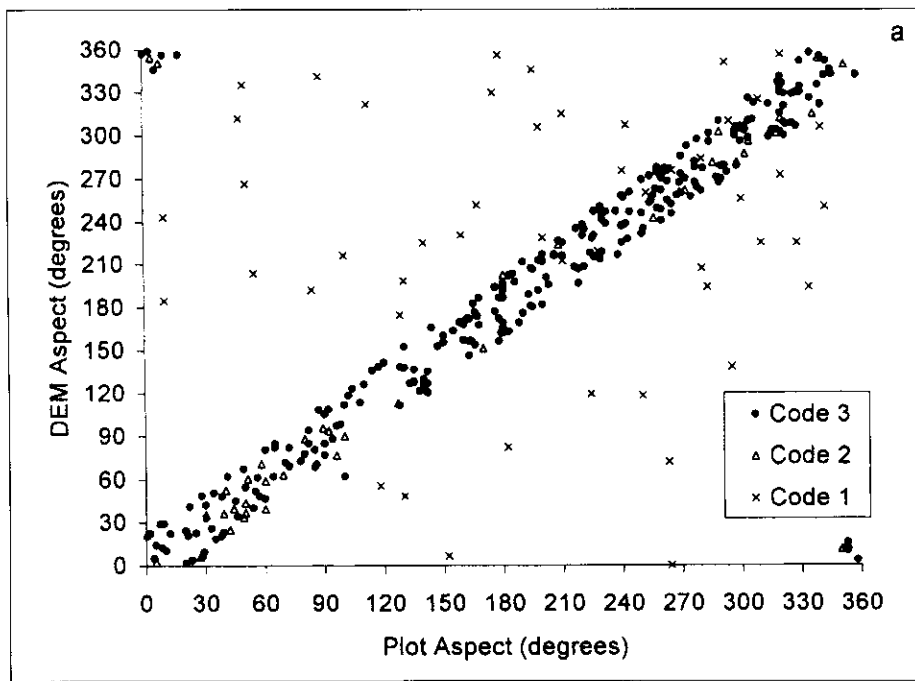


Figure 4a. Relationship between aspect recorded at the original locations in the field and that adjusted with the search routine for a 5 pixel radius window ($r^2 = 0.82$, $\text{DEM Aspect} = 0.92 * \text{Plot Aspect} + 11.4$, $n=391$, $P < 0.0001$)

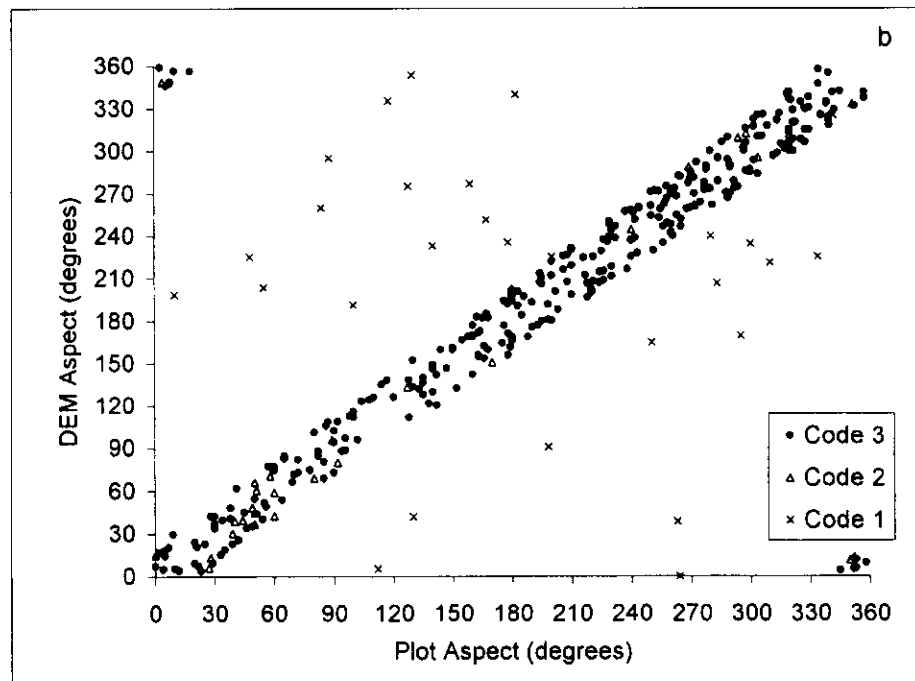


Figure 4b. Relationship between aspect recorded at the original locations in the field and that predicted with a 3 pixel radius window ($r^2 = 0.73$, $\text{DEM Aspect} = 0.85 * \text{Plot Aspect} + 24.1$, $n=391$, $P < 0.0001$)

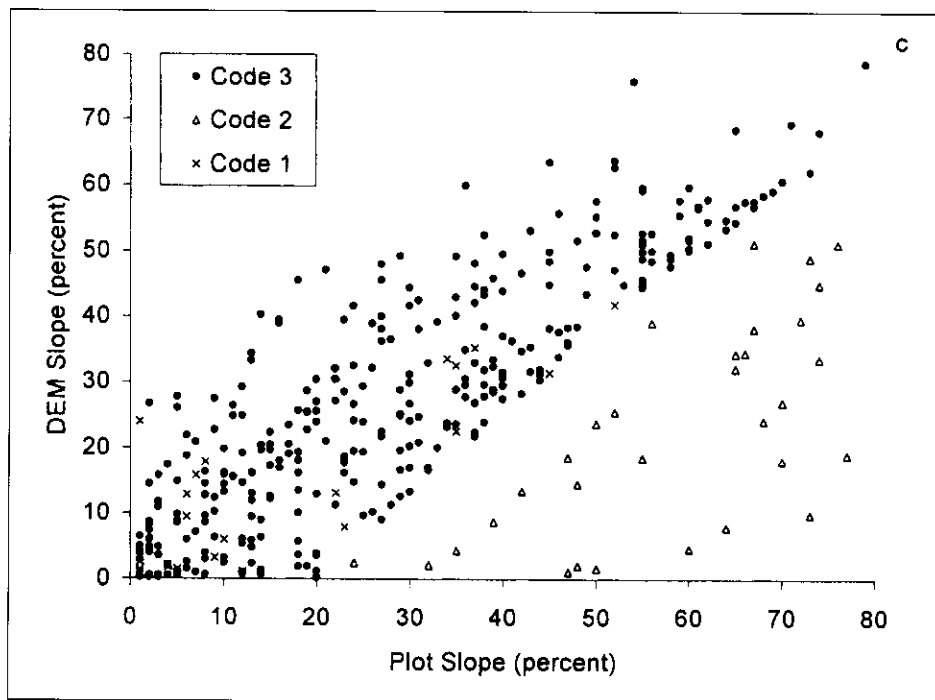


Figure 4c. Relationship between slopes recorded at the original locations in the field and that predicted with a 5 pixel radius window ($r^2 = 0.56$, DEM Slope = $0.67 * \text{Plot Slope} + 6.53$, $n=391$, $P < 0.0001$).

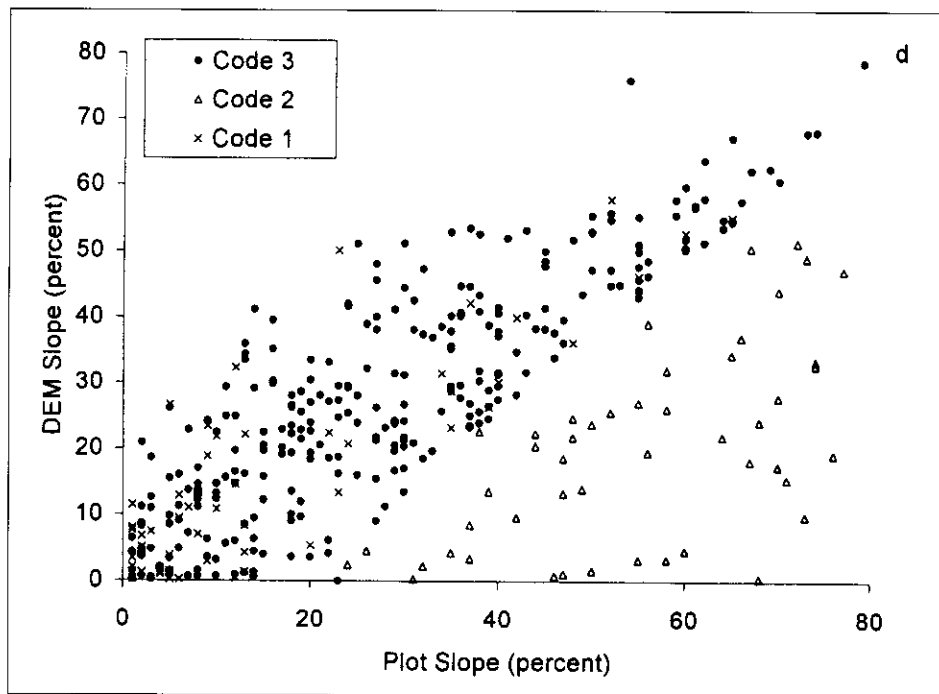


Figure 4d. Relationship between slopes recorded at the original locations in the field and that predicted with a 3 pixel radius window ($r^2 = 0.47$, DEM slope = $0.58 * \text{Plot Slope} + 7.85$, $n=391$, $P < 0.0001$).

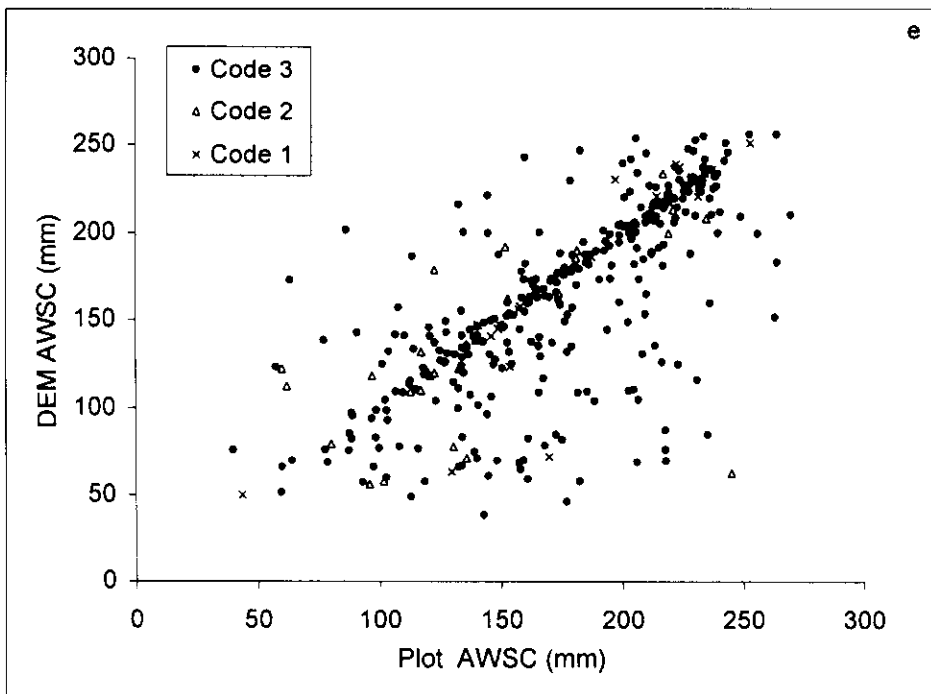


Figure 4e. Relationship between θ recorded at the original locations in the field and that predicted with a 5 pixel radius window ($r^2 = 0.54$, DEM $\theta = 0.63 * \text{Plot } \theta + 69.5$, $n=391$, $P < 0.0001$)

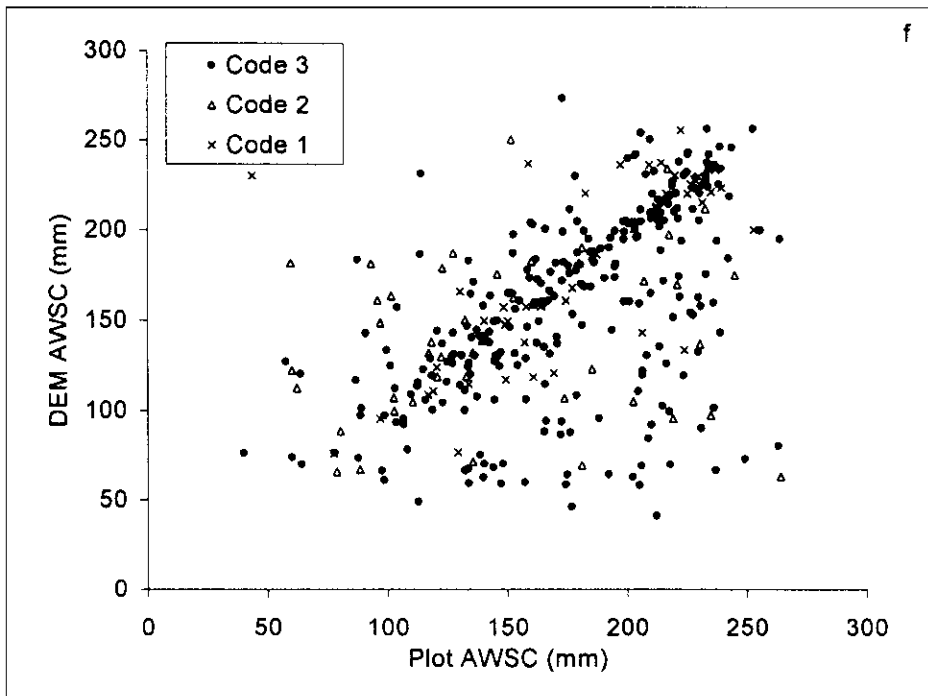


Figure 4f. Relationship between θ recorded at the original locations in the field and that predicted with a 3 pixel radius window ($r^2 = 0.27$, DEM $\theta = 0.47 \text{ Plot } \theta + 98.4$, $n=391$, $P < 0.0001$)

percentage of plots that produced a code 1 (aspect incorrect, slope correct) (15% for the 5 pixel filter and 8% for the 3 pixel filter) indicates that the most of the plots more easily fell within the slope threshold than with the aspect thresholds.

Figure 4c and d indicate that, like the aspect comparison, there is a significant improvement in the agreement between measured slope and that extracted at the new locations from the DEM. The wider search window provides a slightly closer matching of the field observations with those derived with the DEM. With wider window, the codes 2 and code 1 assignments are also less frequent. The effect of topographic smoothing at 100m spatial resolution can be seen with an overall bias; a field-measured slope of 80% corresponds to approximately 70% on the 100m DEM.

Figure 4d and e show the relationship between the measured θ and that predicted by the DEM at the new cell positions using the search algorithm for both the 5 and 3 pixel boxcar windows. The results, as expected, are similar to the slope and aspect analysis with significantly improved rela-

tionships. The search with a 5-pixel radius produced a significantly tighter correspondence with the plots than that with a 3-pixel radius. This is expected as the algorithm in its final step attempts to minimize the difference between field estimates and modeled θ over all the cells with the maximum code value. Because the 5-pixel radius has a larger number of cells, a tighter relationship between the observed and predicted values results. There appears to be no significant pattern in the location of the code 2 or code 1 values in these figures. Overall, model predictions tend to underestimate θ values recorded in the field.

Figure 5 shows statistics on the distances required to move the original plot positions to locations where terrain attributes are in closer agreement. The distributions are shown for both the 3- and 5-window searches. Details of the distances can be seen in Table 3. Overall, the mean movement of the plots to their new location using the 5-pixel radius search window was 435 m and with the 3-pixel radius, 289 m (Table 3).

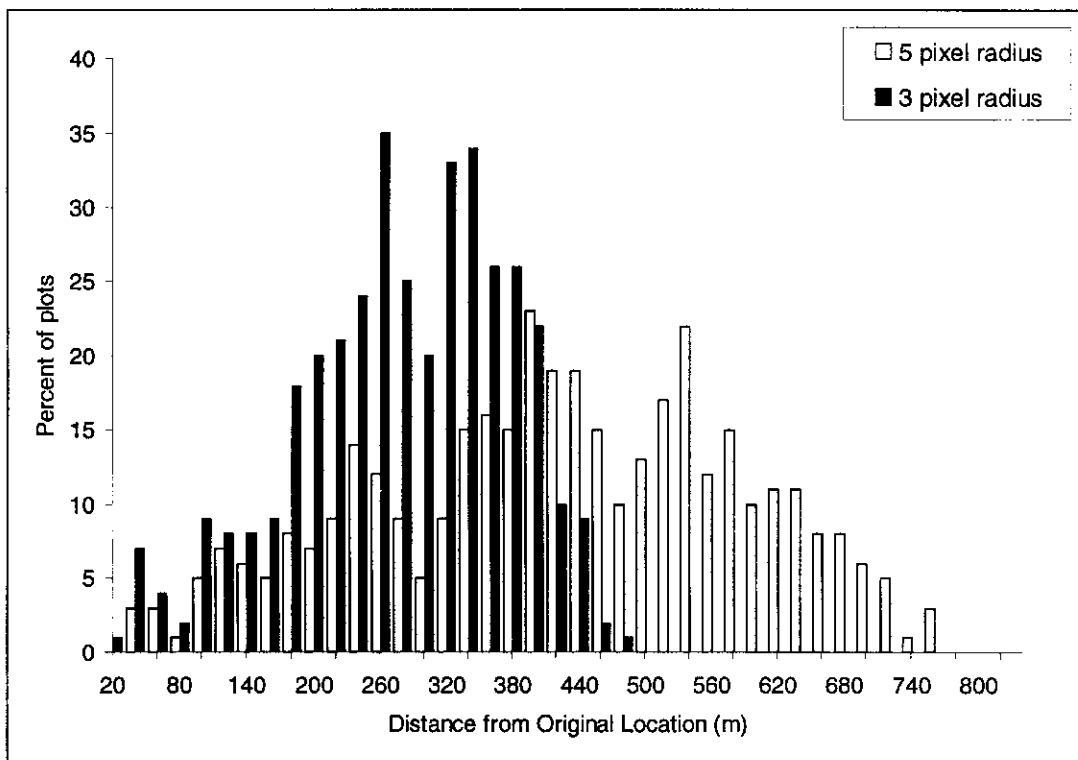


Figure 5. Histogram of distances moved from original locations of plots using 5 and 3 pixel radius windows respectively.

TABLE 3. Summary of distance statistics related to repositioning field plots using hierarchical search routine with two window sizes.

Size of Search Radius (pixels)	Maximum Distance (m)	Minimum Distance (m)	Mean Distance (m)	Variance of Distances (m)
5	749	25.5	412	165
3	461	14.8	269	95

Discussion

The hierarchical-search approach presented here provides an approach of repositioning plots, whose position was originally determined on different base maps and without access to global positioning technology. The approach relies on utilizing the large number of topographic and physiographic datasets that usually accompany field surveys.

As described in the introduction, DEMs are rarely without error and are often unavailable at the most appropriate scale (Hutchinson 1999). An inherent assumption of this technique is that the terrain attributes extracted from the DEM are realistic representations of the local terrain. Finer scale resolution DEM are currently becoming available over the continental U.S. with spatial resolutions of 30 m. Obviously, the techniques developed in this paper can be applied to these fine scale DEMs. An added benefit of utilizing these finer scale DEMs is the more accurate representation of fine scale topographic features such as slopes and gullies.

Given potential errors in both field location of plots and in the interpolation from DEM surfaces, the approach described in this paper provides a link between the two types of data sets by positioning the plots on the DEM, not by their absolute geographic locations but by attempting to match their recorded terrain environment as closely as possible. In many cases where extrapolation of climatic data and modeling of growth and distribution are involved, the actual geographic po-

sition of a plot is generally not as relevant as ensuring that the environmental regimes, which are correlated with terrain attributes, are similar. In the case of solar radiation, the aspect and slope are particularly critical, because assignment of a north slope to a south aspect with 25° slope at 45° Latitude results in a difference of more than 250%. In such cases, the actual plot position on the DEM may be some hundreds of meters from the originally recorded plot position without introducing significant errors in modeling.

Acknowledgements

Dr David Hann was principally responsible for the collection, collation, and maintenance of the extensive forest plot dataset. I thank Dr Hann for allowing access to the dataset and for his willingness to provide additional data when required and comments of the manuscript. Mr. Stephen Brown labored long and hard in preparing the DEM for analysis. His professionalism and help was greatly appreciated. I express thanks to Richard Waring, Mr. Phil Hurvitz, and an anonymous reviewer for constructive criticism on early drafts of this paper.

This research was undertaken at Department of Forest Science, Oregon State University, Oregon while the author was on leave from CSIRO Forestry and Forest Products, Australia. The research was supported by funds from the National Aeronautics and Space Administration (NASA) on Grant NAG5-7506.

Literature Cited

- Band, L.E. 1986. Topographic partition of watersheds with digital elevation models. *Water Resources Research* 22:15-24.
- Band, L.E., Peterson, J.R., Nemani, R. and S.W. Running. 1993. Ecosystem processes at the watershed scale: incorporating hill-slope hydrology. *Agricultural and Forest Meteorology* 63:93-126.
- Beven, K.J. and M. I. Kirkby. 1979. A physically based, variable contributing area model of basin hydrology. *Hydrological Science Bulletin* 24:43-69.
- Beven, K.J. and E. F. Wood. 1983. Catchment geomorphology and the dynamics of runoff contributing areas. *Journal of Hydrology* 65:139-158.
- Binley, A. and Beven, K. 1992. Three-dimensional modeling of hillslope hydrology. *Hydrological Processes* 6: 347-359.

- Bloschl, G. and Sivaplan, M. 1995. Scale issues in hydrological modeling: a review. *Hydrological Processes* 9: 313-330.
- Burrough, P.A. 1986. Principles of geographical information systems for land resources assessment. Clarendon Press, Oxford.
- Franklin, J.F. and C.T. Dyrness. 1973. Natural Vegetation of Oregon and Washington. USDA Forest Service General Technical Report PNW-8. Portland, Oregon.
- Gessler, P.E., McKenzie, N.J. and Hutchinson, M.F. 1996. Progress in soil-landscape modeling and spatial prediction of soil attributes for environmental models. Proceedings of the Third International Conference/Workshop on Integrating GIS and Environmental Modeling. National Center for Geographic Information and Analysis, Santa Barbara, CA. CD-ROM and World Wide Web, http://www.ncgia.ucsb.edu/conf/SANTA_FE_CD-ROM/main.html.
- Hann, D.W. 1983. Field procedures for measurement of standing trees. Department of Forest Resources. Oregon State University, Corvallis, Oregon.
- Hann, D.W. and M.W. Ritchie 1988. Height growth rate of Douglas-Fir: A comparison of model forms. *Forest Science* 34:165-175.
- Hann, D.W. and C.H. Wang 1990. Mortality equations for individual trees in the mixed conifer-zone of southwest Oregon. Forest Research Laboratory, Oregon State University, Corvallis, Oregon. Research Bulletin 67.
- Hann, D.W. and D. R. Larsen 1991. Diameter growth equations for fourteen tree species in southwest Oregon. Forest Research Laboratory, Oregon State University, Research Bulletin 69. Corvallis, Oregon..
- Hutchinson, M.F. 1999. Modelling spatial and temporal variability of climate and terrain. <http://cres20.anu.edu.au/hydweb/hutch/hutch2.html>.
- Jenson S. K. and J. O. Domingue. 1988. Extracting topographic structure from digital elevation data for geographic information system analysis. *Photogrammetric Engineering and Remote Sensing* 54:1593-1600.
- Kirkby, M.J. and D.R. Weyman. 1974. Measurement of contributing area in very small drainage basins. Seminar Paper Series B. No. 3. Dept. of Geography, University of Bristol.
- Kolmogorov A. 1941. Confidence limits for an unknown distribution function. *Annals of Mathematics and Statistics*.12:461-63.
- Mark, D.M. and F. Csillag. 1990. The nature of boundaries on "Area-Class" maps. *Cartographica* 27: 65-68.
- Moore, I. D., R. B. Grayson, and A. R. Ladson. 1991. Digital terrain modelling-a review of hydrological, geomorphological and biological applications. *Hydrological Processes* 5:3-30.
- Nemani, R.R., Running, S.W., Band, L. and D. Peterson. 1993. Regional hydro-ecological simulation system: An illustration of the integration of ecosystem models in GIS. Pages 296-304 *In* M.F. Goodchild, B.O. Parks and L.T. Steyaert (editors) *Environmental Modeling with GIS*. Oxford University Press, New York.
- Running, S.W., Nemani, R.R., Peterson, D.L., Band, L.E., Potts, D.F., Pierce, L.L. and M.A. Spanner. 1989. Mapping regional forest evapotranspiration and photosynthesis by coupling satellite data with ecosystem simulation. *Ecology* 70:1090-1101.
- Running, S.W. 1994. Testing FOREST-BGC ecosystem process simulations across a climatic gradient in Oregon. *Ecological Applications* 4:238-247.
- Singer, M.J. and D.N. Munns. 1987. *Soils: An introduction*. Macmillan publishing company, New York.
- StatSoft Inc. 1995 *STATISTICA for Windows* [Computer program manual]. StatSoft Inc., 2300 East 14th Street, Tulsa, Oklahoma.
- United States Department of Agriculture. 1991. State Soil Geographic Data Base (STATSGO). Soil Conservation Service, Miscellaneous Publication No. 1492. Washington D.C.
- Waring, R.H., and S.W. Running. 1998. *Forest ecosystem analysis: analysis at multiple scales*. Academic Press, San Diego, California.
- Whittaker, R.H. 1960. Vegetation of the Siskiyou mountains, Oregon and California. *Ecological Monographs* 30: 279-338.
- Zeveloff, L. W., and C. R. Thorne. 1987. Quantitative analysis of land surface topography. *Earth Surface Processes and Landforms* 12: 47 - 56.
- Zhang, W. and D.R. Montgomery. 1994. Digital elevation model grid size, landscape representation, and hydrologic simulation *Water Resources Research* 30:1019-1028.
- Zheng, D., Hunt, E.R., and S.W. Running. 1996 Comparison of available soil water capacity estimated from topography and soil series information. *Landscape Ecology* 11:3-14.

Received 17 August 1999

Accepted 17 February 2000